Journal of Cleaner Production 382 (2023) 135280

Contents lists available at ScienceDirect

Journal of Cleaner Production

journal homepage: www.elsevier.com/locate/jclepro

Experimental study on the thermal properties of pigmented mortars for use in energy efficiency applications

Jorge López-Rebollo [a,*], Susana Del Pozo [a], Ignacio Martín Nieto [a], Cristina Sáez Blázquez [a,b], Diego González-Aguilera [a]

[a] Department of Cartographic and Land Engineering. University of Salamanca, Higher Polytechnic School of Ávila, Hornos Caleros, 50, 05003, Ávila, Spain
[b] Department of Electric, System and Automatic Engineering, Universidad de León, León, Spain

ARTICLE INFO

Keywords:
Pigmented mortar
Thermal properties
Heat storage
Solar simulator

ABSTRACT

This study aims at investigating the application of pigments on mortars and evaluating how it affects their thermal properties. In addition, it was analysed whether the addition of this type of substance affects the mechanical and optical properties of the mortars. For this purpose, several mortar samples were made with grey and white cement to which different concentrations of black and white pigment were added. The mechanical characterization tests showed that the compressive strength is not affected by the addition of pigments in the proportions supplied. On the other hand, the thermal conductivity tests also showed a negligible relationship between the proportion of pigment added and the change in the mortar conductivity. Then, the thermal behaviour of these mortar samples subjected to heating with a low-cost solar simulator was also monitored. Results revealed a significant increase in temperature for the mortar samples with black pigments, while those with white pigments barely reduced this temperature. Finally, after performing a spectral reflectance test, a correlation was found between the reflectivity of the pigmented mortars in the optical spectrum and their thermal behaviour.

1. Introduction

The excessive consumption of resources and the generation of a large amount of waste in the construction industry point to the need to use materials with properties that allow their full potential to be exploited in a sustainable way. The inclusion of capabilities on construction materials that go beyond their mechanical properties necessary to ensure the integrity of structures, is a challenge faced by this sector. One of the development paths in the concrete market, accompanied by numerous investigations on its characteristics and capabilities, is the suitability of its use in a recycled manner (Verian et al., 2018; Matias et al., 2020; Teijón-López-Zuazo et al., 2021). One of the recent lines of research is based on the introduction of self-healing capabilities in construction materials (Gupta and Naval, 2020). This line aims to increase the safety and durability of structures that are difficult to monitor and/or maintain. Finally, it is necessary to mention those research lines that analyse the thermal capacities of construction materials on which the present work is focused (Basha et al., 2020; Sukontasukkul et al., 2019).

The thermal requirements in construction materials are beginning to gain importance within the framework of the environmental and energy transition policies adopted by many countries. Among others, the possibilities of improving the performance of air conditioning systems based on the selection of construction materials, means that a great development of this type of solutions is expected in the future. It is also worth mentioning the importance that the thermal properties of construction materials have, for example, in the generation of heat islands that occurs in many urban centres mainly during the summer season (Deilami et al., 2018). An adequate modification of the thermal properties of the concrete could contribute to significantly mitigate this undesirable effect. On the other hand, in certain climatic scenarios, the opposite action can result in an energy advantage. For example, managing to improve the thermal capacities of concrete to increase its energy storage capacity can result in significant savings in the heating systems used (Xaman et al., 2019).

As for granting certain thermal capacities to construction materials, it entails using different additives capable of conferring them the desired

* Corresponding author.
E-mail addresses: jorge_lopez@usal.es (J. López-Rebollo), s.p.aguilera@usal.es (S. Del Pozo), nachomartin@usal.es (I. Martín Nieto), u107596@usal.es (C. Sáez Blázquez), daguilera@usal.es (D. González-Aguilera).

https://doi.org/10.1016/j.jclepro.2022.135280
Received 5 July 2022; Received in revised form 31 October 2022; Accepted 21 November 2022
Available online 24 November 2022

properties without affecting their mechanical properties. The economic, environmental and safety considerations on these additives are an important part of the investigation. In this sense, numerous pigments have been tested with very diverse compositions (Cellat et al., 2019; Berktas et al., 2020; Nocuń-Wczelik and Stolarska, 2019).

The main developments focused on improving the thermal capabilities of construction materials are focused on the use of paint coatings made of Near Infrared (NIR) reflective pigments (Rosati et al., 2021; Divya and Das, 2021), which allow the temperature of buildings to be reduced by applying them to façades and roofs (Puesan and Mestre, 2017). So far, the introduction of pigments as additives for mortars or concrete has been done mainly for architectural and visual design purposes (Corinaldesi et al., 2012), while its addition to other materials, such as asphalt, has been shown to be effective in considerably reducing the temperatures reached without affecting its performance (Badin et al., 2020, 2021). In this sense, the addition of pigments as additives hardly affects the mechanical performance of the mortars, as some research has shown that the differences in their mechanical properties are very slight (Heerah et al., 2021).

Nevertheless, there is a lack of knowledge regarding the thermal performance of this type of mortars with pigmented additives, as research in this field is very scarce and therefore the use of multidisciplinary techniques is presented as an opportunity to study their thermal behaviour.

Traditionally, the improvement of the thermal properties of mortars has been tested from the point of view of thermal conductivity (Corinaldesi et al., 2011; Yun et al., 2013). Thermal conductivity can be measured by applying the infinite line heat source model (Healy et al., 1976) from the heating/cooling process undergone by the samples (Lockmuller et al., 2004). However, from a thermographic point of view, some studies on NIR reflective coatings have shown the feasibility of measuring surface temperature with thermal imaging (Thejus et al., 2021). In this case, the active thermography (Lizaranzu et al., 2015) applied by means of a solar simulator is intended to reveal the difference between the materials due to the alteration of thermal diffusivity and heat flow caused by their composition (Maldague, 2001). The use of solar simulators is widespread in the field of renewable energies, and more specifically to carry out performance tests on solar thermal and photovoltaic systems (Tawfik et al., 2018). There is an extensive review on the types of solar lamps and their performance (Colarossi et al., 2021) as well as on the use of low-cost solar simulators for multiple applications (Tawfik et al., 2018; Colarossi et al., 2021; Codd et al., 2010; Meng et al., 2011).

Together with thermal conductivity and thermographic analysis, the use of optical spectrum sensors allows the analysis of the radiation absorbed/reflected by the samples and has been used in many works to study this type of behaviour in other construction materials, generally related to heritage (Sánchez-Aparicio et al., 2018; Del Pozo et al., 2016; Rodriguez-Gonzalvez et al., 2015). For this purpose, multi and hyperspectral imaging (Santos et al., 2018; Bonifazi et al., 2018) are other widely used techniques while spectroscopy (Reuben et al., 2018; Watanabe et al., 2019; Florian, 2022) allows to reach the highest level of detail given its precision and resolution.

As consequence, this work aims to advance in the knowledge of the thermal behaviour of pigmented mortars through the application of multidisciplinary techniques to study their thermal properties and their heating and cooling performance. To this end, an experimental campaign is carried out on mortars with different dosages of pigment using thermal, optical and mechanical tests. After this Introduction Section, the materials and the description of the techniques employed are described in the Materials and Methods (Section 2). In Section 3, the experimental results for each test are shown, the connections between the results of the different thermal tests are analysed and some explanations are proposed. Finally, in Section 4, a series of conclusions are exposed, some of which were expected (the addition of pigments in the percentages established does not affect the compressive strength of the mortar), while others are promising for the construction and building sector and open new engaging research lines.

2. Materials and methods

This work focuses on the use of additives particularly designed to alter the colour of cement and, specifically, on the study of their effect on the thermal properties of mortars. In addition to this study, it has been considered to evaluate the conservation of its mechanical properties and to analyse the influence they have on the reflectance in the optical spectrum (visible and infrared).

To carry out these tests, two different types of cement (grey and white) have been used, which different proportions of white and black pigments have been added in order to study the effects of the pigmentation on its mechanical, thermal and optical properties. With these pigmented cements, and following the procedure described in the following subsections, mortars have been prepared to produce the samples on which the following tests have been performed. Fig. 1 shows a scheme of the workflow followed.

- Mechanical characterization. In order to verify whether the mechanical properties are maintained or whether the addition of pigments has any effect on their behaviour, compressive strength tests were carried out.
- Thermographic analysis. The active thermography applied allows analysing the thermal behaviour of the sample against heating and cooling processes, so that a continuous monitoring of its surface temperature is carried out.
- Optical reflectivity test. To analyse the radiation absorbed/reflected by the mortar samples in the optical spectrum, a Terrestrial Laser Scanning (TLS) operating in the NIR spectrum (at 905 nm) with an integrated Red-Green-Blue (RGB) camera was used.
- Thermal conductivity test. The main objective is to study the possible connections between the variations in thermal conductivity from the different samples, with the results obtained in the other tests carried out. In addition, the test will reveal if the different dosages of pigments in the mortars could have an effect on this thermal parameter.

2.1. Materials for the pigmented mortars

Pigmented mortars are mostly used for functional and aesthetic applications buildings, so their mechanical behaviour is not a limiting factor for their manufacture, though it is advisable that its properties and durability remain unchanged. They have a dosage made up by of water, natural siliceous aggregates, Portland cement and chemical additives such as pigments in this case. Within the scope of this study, the focus was on evaluating the use of different dosages of pigment and its influence on the properties of mortars. In order to analyse the thermal behaviour and achieve notable differences, two types of cement and two types of pigment were used on this research. The fine natural aggregate used in all the mixes was silica sand, 0–4 mm fraction. No additives other than pigment were used.

On the one hand, the blinder used for manufacturing the grey mortar was a cement type BL II/B-LL 32.5 R. This Grey Cement (GrC) has the following components: i) a Clinker content comprised between 65 and 79%; ii) a Limestone content of 21–35%; iii) a Chloride content: ≤ 0.10; iv) a Sulphate content: ≤ 4.0; and v) a soluble toilet chromium VI content $\leq 0.0002\%$. It has a beginning of setting: ≥ 60 min and an end of setting: ≤ 720 min. The expansion is less than 10 mm. Resistance at 28 days ≤ 32.5 MPa.

On the other hand, White Cement (WhC) with a whiteness content $\geq 85\%$ was chosen, looking for the best contrast with the dark pigment dosages. This cement is type BL II/B-LL 42.5 R and its composition is similar to that of GrC. In this case, resistance at 28 days ≤ 42.5 MPa.

Regarding the pigments, white and black dyes were used in different

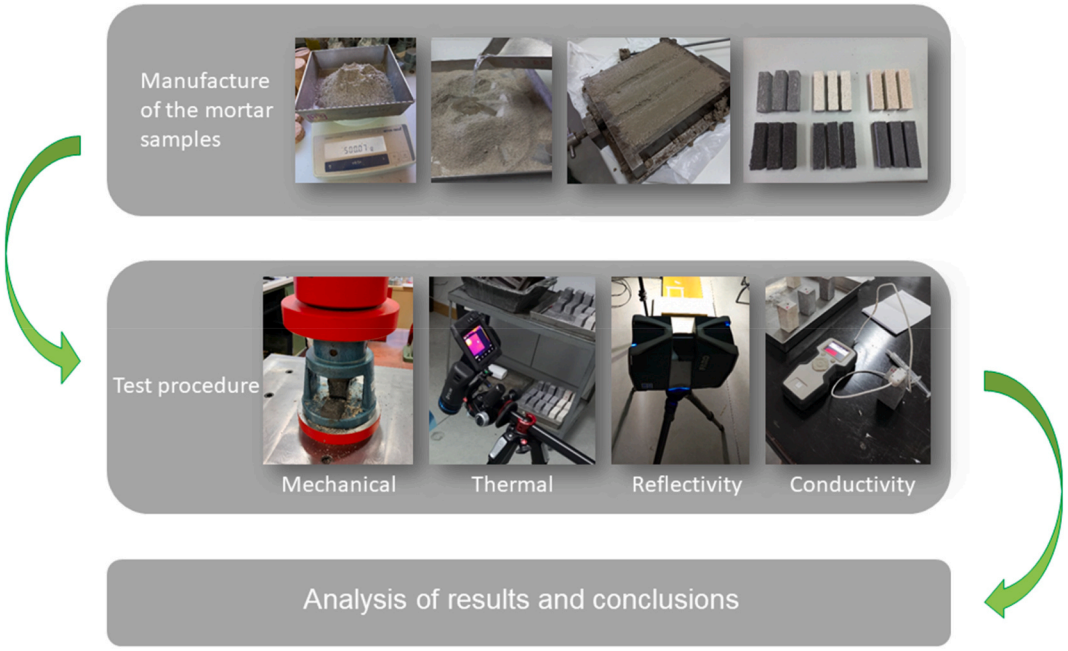

Fig. 1. Workflow scheme for the mechanical, thermal and physical characterization of pigmented mortars.

proportions (Table 1). The White Pigment (WhPig) used belongs to Oxined® and the Black Pigment (BlPig) used belongs to HobbyColor. Both contain synthetic metal oxides, inorganic, insoluble in water, resistant to alkalis and unaltered by the effect of sunlight and any other atmospheric agent.

A total of 12 mortar samples were made with the same proportions of sand (3), cement (1) and water (0.5), so that only the amount of pigment was modified. A high percentage of pigment was used in order to achieve greater coloration, so that 10% corresponding to the weight of the cement was added. Although the proportions of each pigment were varied in each specimen, the same total weight was maintained in each sample, except in the reference ones (G5-Ref and W5-Ref).

2.2. Mechanical characterization

With the aim of verifying the influence of the pigment on the mechanical properties, mechanical characterization tests were carried out. These tests allow us to know if the strength of the mortar increases or decreases depending on the type and amount of pigment for each of the dosages with respect to the reference. The mortar solutions were evaluated by means of compression tests according to guideline UNE-EN 196-1 (AENOR. UNE-EN). In order to carry out these tests, an electromechanical test machine Servosis ME-405/50/5 was used with a load cell of 500 kN and the corresponding compression plates. It was necessary to use an auxiliary device (Fig. 2) to carry out the compression tests on specimens with standardized dimensions. This device consists of two 40 × 40 mm plates on which the sample is placed, so that the upper plate of the machine transmits the load to the upper plate of the device by means of a spherical joint.

The specimens for the mechanical characterization were manufactured following the guideline UNE-EN 196-1. Initially, moulds to manufacture three 160 × 40 × 40 mm specimens were used for each of the mixtures. The specimens were kept for 24 h in the moulds in conditions of 20 ± 2 °C and relative humidity greater than 90%. Subsequently, the moulds were removed, and the specimens were kept in water at a temperature of 20 ± 2 °C until reaching 28 days of curing.

In order to reduce and adapt the dimensions to the regulations, each of the specimens was cut, obtaining two semi-prisms of approximately 80 mm in length. In this way, one of the halves was used for the compression tests while the other half was reserved for the rest of the tests.

Table 1
Pigment proportions of each mixture.

Nomenclature	Cement Colour	BlPig (g)	WhPig (g)
G1	Grey	50	0
G2	Grey	37.5	12.5
G3	Grey	25	25
G4	Grey	12.5	37.5
G5-Ref	Grey	0	0
G6	Grey	0	50
W1	White	50	0
W2	White	37.5	12.5
W3	White	25	25
W4	White	12.5	37.5
W5-Ref	White	0	0
W6	White	0	50

2.3. Thermographic analysis

With the objective of carrying out a thermographic analysis to

Fig. 2. Test Machine and auxiliary device.

determine the behaviour of the mortars, the active thermography technique and the step heating was used. This method consists of applying heat to the specimens by means of a lighting system under controlled conditions and for a certain time, so that their heating and cooling phases can be monitored. This monitoring was carried out with equipment made up of: i) a thermographic camera FLIR T540; and ii) a lighting system with a low-cost solar simulator.

In this case, the FLIR T540 camera with a 42° lens was used, which allows a field of view of 42° × 32°. The camera has an infrared resolution of 464 × 348 pixels in addition to incorporating a 5 MPx visible sensor that allows both images to be superimposed. It also has a laser sensor to measure the distance to the object and perform autofocus. It has a thermal sensitivity <30 mK at 30 °C and is calibrated for a temperature range of −20 to 120 °C. Finally, it allows a shooting speed of 30 frames per second. The acquisition of images was carried out using FLIR ResearchIR software, which allows us to configure test parameters and environmental conditions, as well as defining image capture protocols.

Considering that the mortars are intended to be used in real environmental conditions, an attempt was made to use a solar simulator that could resemble as much as possible the heating produced by the sun's rays. The lighting system consists of a developed low-cost solar simulator (Fig. 3). The most widely used lamps to create solar simulators are usually argon arc, metal halide, tungsten halogen or xenon arc (Tawfik et al., 2018; Colarossi et al., 2021). In this case, a 250 W metal arc halide lamp (Table 2) was chosen. Thus, the solar simulator consists of a metal halide lamp, a ballast to regulate the continuous flow of the arc and to provide the appropriate voltage to the lamp, a support for the lamp with an aluminium plate to concentrate the radiation, and a sample tray.

Solar simulators are devices capable of approximately simulating, by means of artificial light, the natural light of the sun. Thanks to them, studies and simulations can be carried out under controlled laboratory conditions, guaranteeing a certain stability in environmental conditions. In addition, this type of test allows planning, programming, and taking ad-hoc data, guaranteeing reproducibility and repeatability. As for the main aspects to consider in the design of solar simulators are the spectral correspondence, the uniformity of irradiation and its temporal stability. In this study, the uniformity and temporal stability of the luminous flux received by the samples is guaranteed because they were always located in the same place with respect to the lamp (Fig. 3), in addition to the fact that the heating-cooling tests were carried out under the same conditions (same turn-on and turn-off duration for all simulations). Regarding the optical spectrum, as Fig. 4 shows, metal halide lamps have a spectral coverage close to the global solar radiation spectrum.

2.4. Optical reflectivity test

In order to analyse and quantify the part of radiation reflected by the samples in the Visible (VIS) and NIR spectrum, it was decided to carry out a data acquisition with a Faro Focus 3D 120 terrestrial laser scanner equipped with an integrated RGB camera (specifications are shown in Table 3). This sensor is an active phase shift device that emits electromagnetic radiation (at a wavelength of 905 nm) and collects the reflected back from objects. Thanks to this, not only can objects be reconstructed in three dimensions with millimetric accuracy, but also the intensity reflected from them can be measured. This information will be useful to analyse the amount of radiation absorbed by the mortar samples and, therefore, likely to be subsequently emitted and recorded by the thermographic camera.

2.5. Thermal conductivity test

Thermal measurements were performed using the thermal properties analyser TEMPOS. This device, developed by the commercial group "METERgroup" complies with the ISO 2008 standards and the ASTM 5334 and IEEE 442 and is specifically designed for taking accurate readings of thermal conductivity, thermal resistivity, thermal diffusivity, and specific heat in different types of materials.

For the mentioned readings, different specific needles are used based on the nature of the material and the measuring test. Each needle produces a discrete amount of heat, virtually eliminating the moisture movement (or free convection in the case of liquids) that could influence the reading. In addition, the short heating times required by TEMPOS (around 1 min) allows to measure frozen materials and even fluids (George et al., 2020).

The operation of this equipment is based on the infinite line heat source theory, so the thermal conductivity is obtained by monitoring the dissipation of heat from the needle probe. Heat is inserted to the needle for an established heating time *th*, and temperature is then measured in

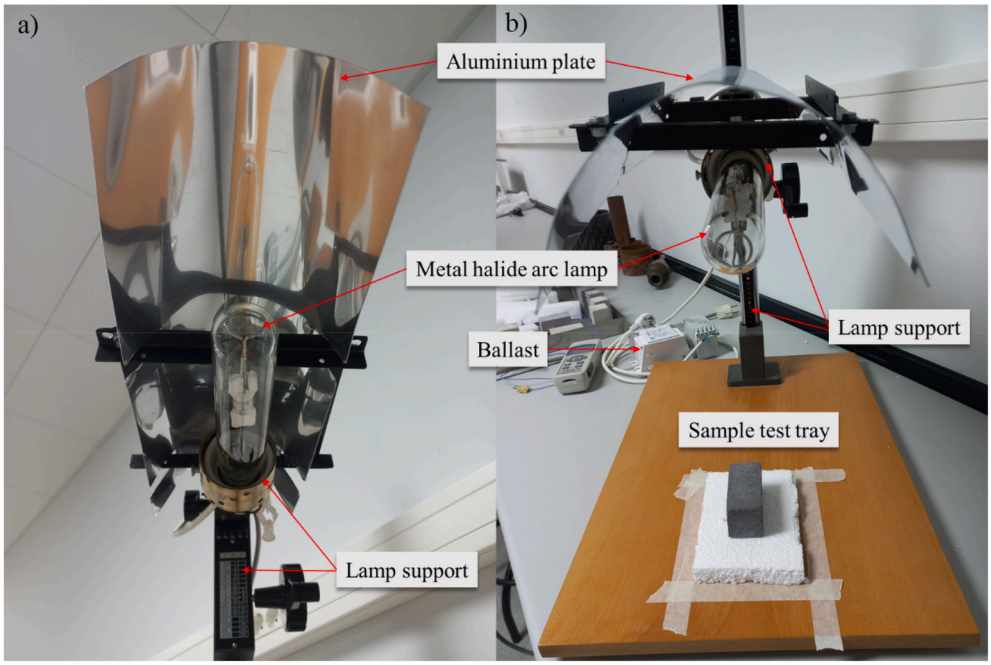

Fig. 3. Low-cost solar simulator device. (a) Bottom view of the lamp and reflective aluminium coating; (b) Configuration of the device together with the test sample.

Table 2
Metal halide arc lamp main features.

Attribute	Value
Product name	HPI-T Plus 250W/645
Nominal luminous flux	19500 lm
Colour temperature	4500 K
Length	255 mm
Diameter	47 mm

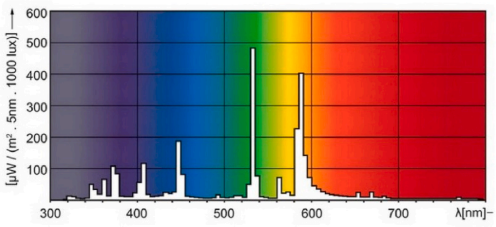

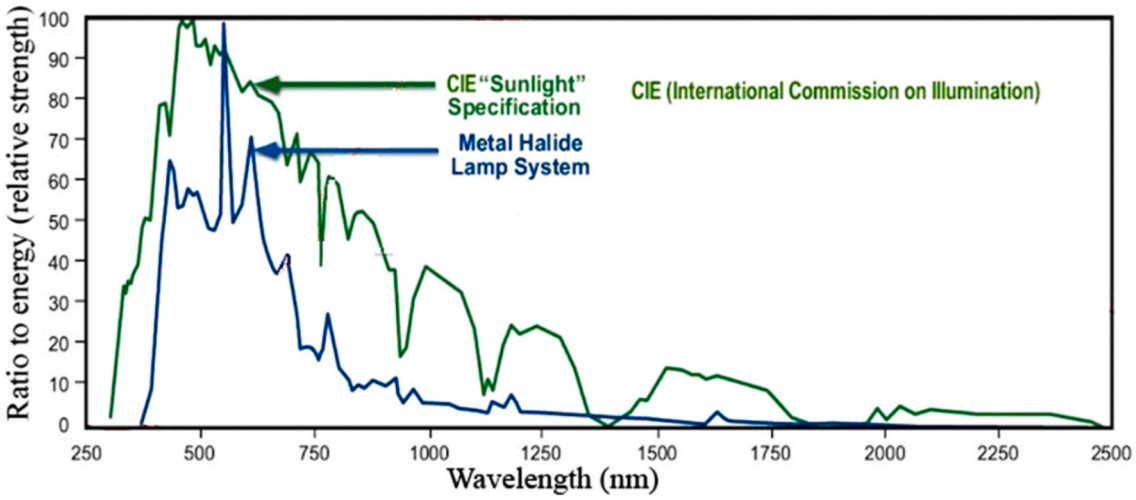

Fig. 4. Spectral distribution chart comparing metal halide lamps with sunlight (PublicLab, 2022).

the monitoring needle during heating and for an extra time equal to *th* after heating (Carslaw and Jaeger, 1959). The following Eq. (1) shows how the temperature during heating is obtained.

$$T = m_0 + m_2 t + m_3 lnt \quad (1)$$

where m_0 is the ambient temperature during heating; m_2 is the rate of background temperature drift; and m_3 is the slope of a line relating temperature rise to logarithm of temperature.

In the same way, the model during cooling is described in Eq. (2).

$$T = m_1 + m_2 t + m_3 \, ln\frac{t}{t - t_h} \quad (2)$$

Finally, the thermal conductivity parameter is calculated from Eq. (3), which also considers the heat flux (q).

$$k = \frac{q}{4m_3} \quad (3)$$

In the case of the present research, conductivity measurements were performed using the RK-3 single needle, conceived for solid and rocky materials. The specifications of this sensor are included in the following Table 4.

Table 3
Faro Focus-3D 120 main features.

Attribute	Value
Physical principle	Phase shift
Wavelength (nm)	905 - near infrared
Measurement range (m)	0.6–120
Field of view (degrees)	360 H × 320 V
Accuracy nominal value at 25 m (mm)	2
Beam divergence (mrad)	0.19
Capture rate (points/s)	122,000/976,000
Radiometric resolution (bits)	11

3. Experimental results

3.1. Mechanical properties

A total of 36 tests were carried out following the guideline UNE-EN 196-1, 18 of which correspond to specimens with grey cement (GrC) (Table 5) and another 18 which correspond to specimens with white cement (WhC) (Table 6). For each type of cement, six different dosages were used (Table 1) and for each of these three specimens were tested. According the guideline UNE-EN 196-1 (AENOR. UNE-EN), the specimens were centred in the plates and the speed test was set at 2400 ± 200 N/s. Taking in account that the dimensions of the plates are 40 × 40 mm, the compressive strength was calculated as follow (Eq. (4)).

$$UCS = \frac{F_c}{1600} \quad (4)$$

where *UCS* is the unconfined compressive strength (Mpa); F_c is the maximum breaking load (N) and 1600 is the area of the plates (mm^2).

Taking into account that the two types of cement have differences in their mechanical properties, the compressive strength analyses were carried out separately, although the procedure was similar in both cases.

Table 4
Specifications of the single needle RK-3 used with TEMPOS device.

RK-3 needle specifications	
Size	3.9 mm diameter x 60 mm length
Range	Resistivity: 17–1000 °C·cm/W
	Conductivity: 0.1–6 W/(m·K)
Accuracy	Conductivity: ±10% from 0.1 to 6 W/(m·K)

Table 5
Results obtained of the mechanical characterization of the grey cement.

Nomenclature	UCS (Mpa)	Dosage Average (Mpa)	Dosage Deviation (%)	Total Deviation (%)
G1-1	29.1	29.1	0.1	0.8
G1-2	28.5		1.9	2.6
G1-3	29.7		2.0	1.2
G2-1	29.1	29.3	0.5	0.6
G2-2	30.0		2.3	2.3
G2-3	28.8		1.8	1.8
G3-1	29.8	29.3	1.7	1.7
G3-2	28.5		2.6	2.6
G3-3	29.6		0.9	0.9
G4-1	27.4	29.1	6.0	6.5
G4-2	30.7		5.2	4.6
G4-3	29.4		0.8	0.3
G5-Ref-1	30.4	31.2	2.6	3.7
G5-Ref-2	29.5		5.4	0.7
G5-Ref-3	33.7		8.0	15.0
G6-1	27.5	27.8	0.9	6.1
G6-2	28.4		2.2	3.1
G6-3	27.4		1.3	6.4

Table 6
Results obtained of the mechanical characterization of the white cement.

Nomenclature	UCS (Mpa)	Dosage Average (Mpa)	Dosage Deviation (%)	Total Deviation (%)
W1-1	43.6	44.8	2.7	3.1
W1-2	44.4		0.9	5.1
W1-3	46.4		3.6	9.8
W2-1	44.6	43.1	3.5	5.6
W2-2	41.7		3.1	1.2
W2-3	42.9		0.5	1.5
W3-1	43.0	41.0	4.9	1.7
W3-2	40.1		2.1	5.0
W3-3	39.8		2.8	5.7
W4-1	39.8	41.7	4.4	5.7
W4-2	42.6		2.2	0.8
W4-3	42.6		2.2	0.8
W5-Ref-1	42.5	43.2	1.6	0.7
W5-Ref-2	43.2		0.1	2.2
W5-Ref-3	43.9		1.6	4.0
W6-1	39.5	39.8	0.5	6.4
W6-2	41.3		3.9	2.2
W6-3	38.4		3.4	9.1

First, the compressive strength was obtained for each of dosages, so that an average value was calculated, as well as the deviations of each of the samples with respect to this mean value. In accordance with the requirements of the guideline, all the values presented deviations of less than ±10%, so the tests can be considered as valid. Next, it was decided to take all the samples as if they belonged to the same group, so the deviation of each one of them with respect to the total mean value was calculated.

The deviations from the total mean value are within the limits ± 10% for each of specimens in both GrC and WhC (Fig. 5, Fig. 6). Only one abnormal value was found that exceeded the upper limit for GrC (G5-Ref-3). This value corresponds to a sample of the reference dosage, which could lead one to think that the application of pigments reduces the compressive strength. Despite this anomaly, the other two values are within limits and are consistent with the rest of samples, being very close to the mean value. In addition, it is worth mentioning that the value that exceeds the limits also has a high deviation (8%) with respect to the values of this same dosage, so it can be taken as a disposable value as it corresponds to a single specimen as indicated in the guideline.

The rest of the GrC specimens as well as all those corresponding to WhC have a similar behaviour, whose deviation falls within the established limits. In addition, the small variations do not seem to have any relationship with the pigment content, since some values are above and others below without a clear trend. These variations may be due to heterogeneities caused in the material by small differences or by human action during the manufacturing or curing stages. In this way, it can be stated that the application of pigments does not have an influence on the compressive strength of this type of mortar.

3.2. Thermal behaviour

3.2.1. Tests setup

For the thermal study, a sample of each dosage was used, so a total of 12 specimens were analysed. The specimens correspond to the remaining semi-prism from the compression tests and their size is 40 × 40 mm with an approximate length of 80 mm.

The tests were carried out individually and under the same conditions, so that the specimens were placed under the solar simulator at a distance of 0.5 m (Fig. 3). In order to avoid heat transfer to the support surface, the samples were placed on a polystyrene panel. The camera was placed at a distance of 0.5 m, focusing on the upper surface of the sample on which the heating is caused. The angle of incidence of the

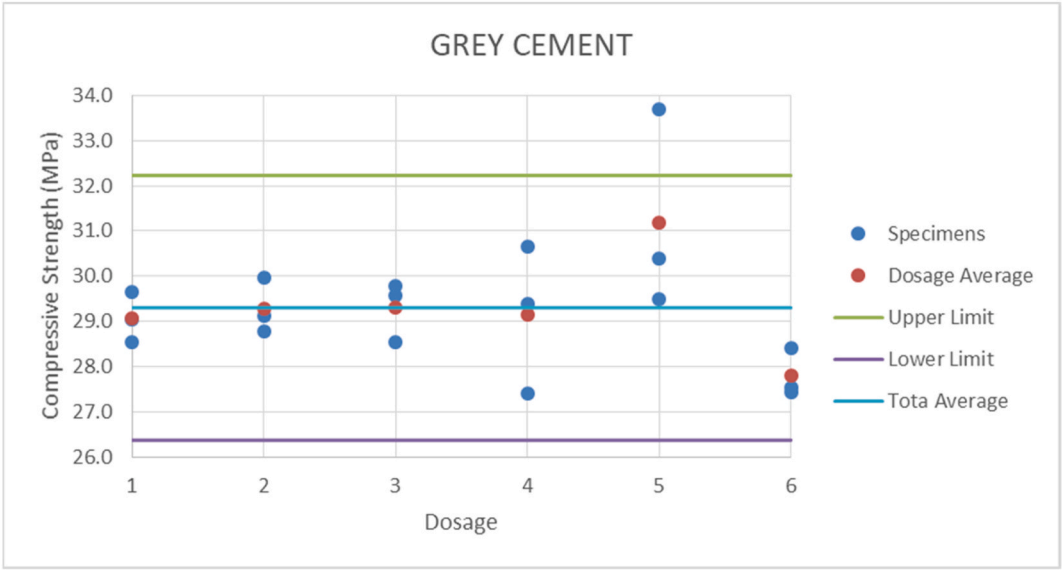

Fig. 5. Compressive Strength and deviation limits of Grey Cement.

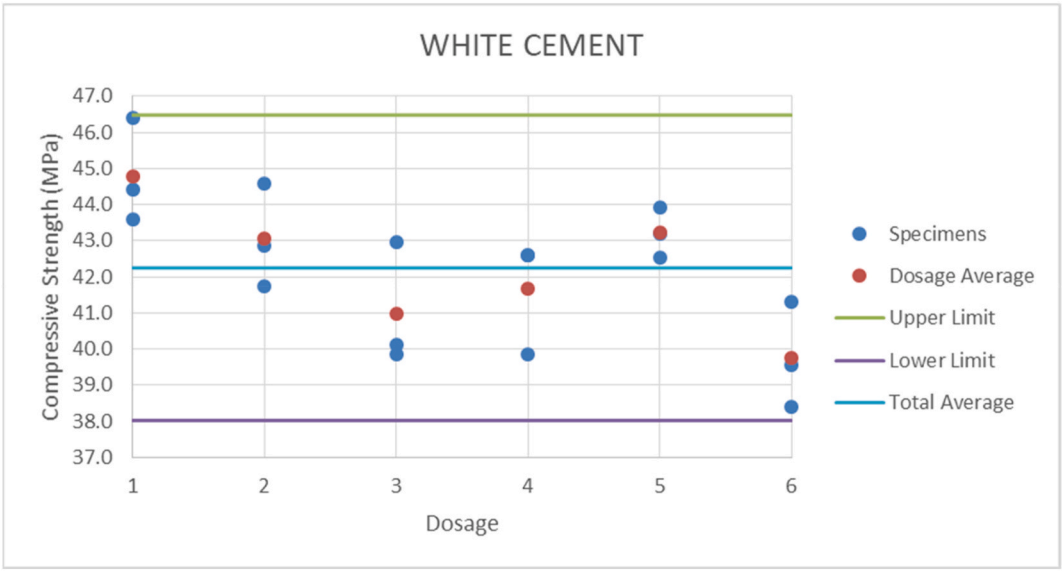

Fig. 6. Compressive Strength and deviation limits of White Cement.

light rays was tried to be as perpendicular as possible, as well as the direction of the camera, which had a slight angle of inclination due to the position of the solar simulator.

In order to all the tests were carried out under the same conditions, the samples were kept isolated at a constant temperature of 23 °C until the start of the tests. Initially, the solar simulator was turned on for 10 min before each test, so that it reached stable illumination. Next, the sample was placed under the simulator, starting the capture of thermographic images while heating for 15 min. Finally, the samples were allowed to cool for 30 min, continuing the acquisition of images. Considering that the time test was long, the thermographic images were acquired every second.

Taking into account that the samples have a reduced size and the edge effect can produce differences between the central zone and the outer zone of the samples, three approaches were carried out for these tests: i) full sample; ii) centre; and iii) edges (Fig. 7). On the one hand, the analysis of the thermographic images was carried out by selecting a rectangular Region Of Interest (ROI) that covered the full sample. In order to determine if the aforementioned edge effects exist, a central ROI, corresponding to a size of 60 × 20 mm, was selected. Finally, the inverse ROI was selected, that is, a rectangle corresponding to the full sample in which the inner ROI selected in step 2 is extracted.

3.2.2. *Thermal results*

For each of the tests and their corresponding approach, a similar procedure was carried out to extract the maximum temperature increments for the selected ROI in the samples. First, the average temperature value of the ROI was calculated for each of the frames, which made it possible to eliminate the pixels with anomalous values and thus eliminate the errors of a punctual nature. Then, the heating and cooling curves were obtained with a total of 2700 points corresponding to each of the images acquired in the test (Fig. 8, Fig. 9). To reduce the noise of the curve due to the sensitivity of the camera, a moving average filter was applied to smooth the curve and eliminate the peaks produced by those frames that could present anomalous values. Finally, the maximum temperature increases (Table 7, Table 8) were obtained from these curves, which correspond to the time immediately prior to switching off the solar simulator.

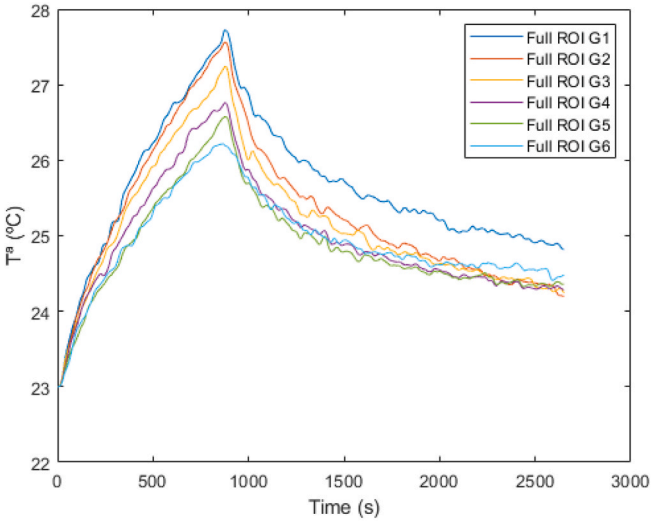

Fig. 8. Heating and cooling curves of Grey Cement.

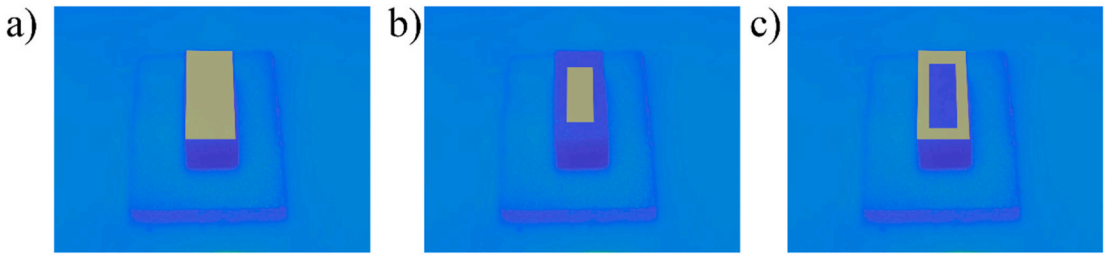

Fig. 7. Region Of Interest for each of the approaches. a) Full sample. b) Centre. c) Edges.

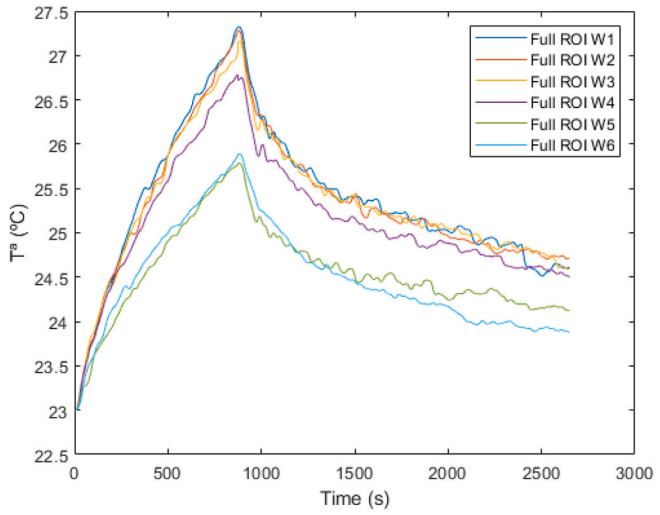

Fig. 9. Heating and cooling curves of White Cement.

Table 7
Temperature increments (°C) for each ROI of Grey Cement.

Nomenclature	Full ROI	Centre ROI	Edge ROI
G1	4.73	4.75	4.71
G2	4.57	4.6	4.55
G3	4.24	4.28	4.21
G4	3.77	3.78	3.75
G5-Ref	3.58	3.59	3.57
G6	3.22	3.22	3.21

Since the differences between each of ROIs were minimal, it can be considered that the edges of the samples do not cause any significant heat loss effect, at least during the heating stage. This means that the heating produced with the solar simulator is homogeneous, as the coefficient of variation of the values for each pixel within the Full ROI was approximately 1% for all samples, which can be attributed to the noise produced in the thermographic images. For this reason, it was decided to show only the results corresponding to the Full ROI, as they are representative of the behaviour of the entire sample surface. In order to compare the two types of cement and each of the mixtures manufactured, the results obtained for each of them are shown below (Fig. 10).

Comparing the two types of cement used, it can be seen that, in general, the temperature increase is higher for the samples manufactured with grey cement. However, the colours produced by the different dosages seem to have a significant influence beyond the original colour of the cement.

On the one hand, the higher percentage of BlPig produces a higher temperature increase, so that mortars with full BlPig reach a higher heating. In this sense, for the mortar manufactured with GrC, the samples corresponding to dosage 1 have achieved 32% more heating compared to the reference dosage (5) (Fig. 10). In the case of the mortar manufactured with WhC, the heating corresponding to dosage 1 was 55% higher than the reference dosage (5) (Fig. 10). This temperature increase can be considered as significant and comparable in both cases, taking into account that the mortar with grey cement started from a darker colour.

Table 8
Temperature increments (°C) for each ROI of White Cement.

Nomenclature	Full ROI	Centre ROI	Edge ROI
W1	4.33	4.35	4.31
W2	4.28	4.32	4.23
W3	4.16	4.19	4.14
W4	3.78	3.82	3.75
W5-Ref	2.79	2.81	2.78
W6	2.89	2.89	2.88

However, the full WhPig does not have the same effect on the two types of mortar. While for the mortar manufactured with GrC the temperatures reached are lower with WhPig, for the mortar manufactured with WhC the increase is very similar, even slightly higher in the mixture containing full WhPig. This may be due to the fact that the type of cement used has a high whiteness content, so that the pigment hardly causes any whitening.

The results obtained for full BlPig and WhPig are significant and can be further analysed with the other techniques used in the experimental campaign. Nevertheless, the results for the intermediate mixtures only allow us to know the influence of the pigment type, resulting in intermediate values with less interpretation, as the mixture of the two inverse pigments (BlPig and WhPig) does not generate a proportional and comparable colour.

3.3. *VIS and NIR reflected radiation*

3.3.1. *Tests setup*

The data acquisition with the TLS was perform by one scan as orthogonally as possible to the mortar samples. For the TLS data collection, the 12 mortar samples were placed at such a height that the laser beam hit them as orthogonally as possible, since the geometry of the acquisition affects the backscattered intensity, both distance and angle of incidence. Thus, the samples were placed on a support (Fig. 11) and the TLS was fitted onto a tripod stand so that both the mortar samples and the TLS laser beam were at the same height. The distance between the mortar samples and the TLS was about 5 m.

Regarding the TLS configuration, it was established a spatial resolution of 6 mm at 10 m, enough to extract redundant and representative radiometric information (400 points per mortar sample). In addition, the data acquisition was performed with photorealistic colour thanks to the parallax-free RGB camera of 70 megapixels with 8-bit radiometric resolution that the Faro Focus 3D 120 has integrated.

After data collection, the point cloud with *X, Y* and *Z* coordinates, visual and near infrared radiometric information, was segmented and analysed. Specifically, the median of the digital values of each of the 12 samples was calculated for the 4 wavelengths registered: 450 nm (blue band of the integrated camera), 550 nm (green band of the integrated camera), 650 nm (red band of the integrated camera) and 905 nm (TLS near infrared wavelength). Since the radiometric resolutions of the integrated camera and the laser scanner differ, 8 and 11 bits respectively, the values were normalized to 11 bits to be able to make comparisons and even be able to extract the spectral behaviour of the 12 samples at the visible and near infrared spectrum.

3.3.2. *Reflected radiation analysis*

The analysis of the radiation reflected by the specimens in the visible and near infrared is very important since it explains the energetic behaviour of the samples. Thus, the more radiation reflected in the visible and infrared, the less radiation absorbed and therefore less radiation emitted and vice versa. Thanks to the data collection with the TLS the spectral response of the mortar samples in the visible and near infrared can be extracted (Fig. 12) even though the analysis is carried out at digital levels (11 bits).

In this sense, the mortar samples can be ordered according to their spectral behaviour (Fig. 13) from greater to lesser reflection of radiation in the visible: W6, W5, G6, G5, G4, W4, G3 and W3, G2 and W2, W1, and G1. In the case of its spectral behaviour in the near infrared, the order followed is practically the same: W6, W5, G6, G5, G4 and W4, G3 and W3, G2 and W2, W1 and G1.

Finally, it is worth mentioning that all the mortar samples reflect more radiation in the near infrared than in the visible.

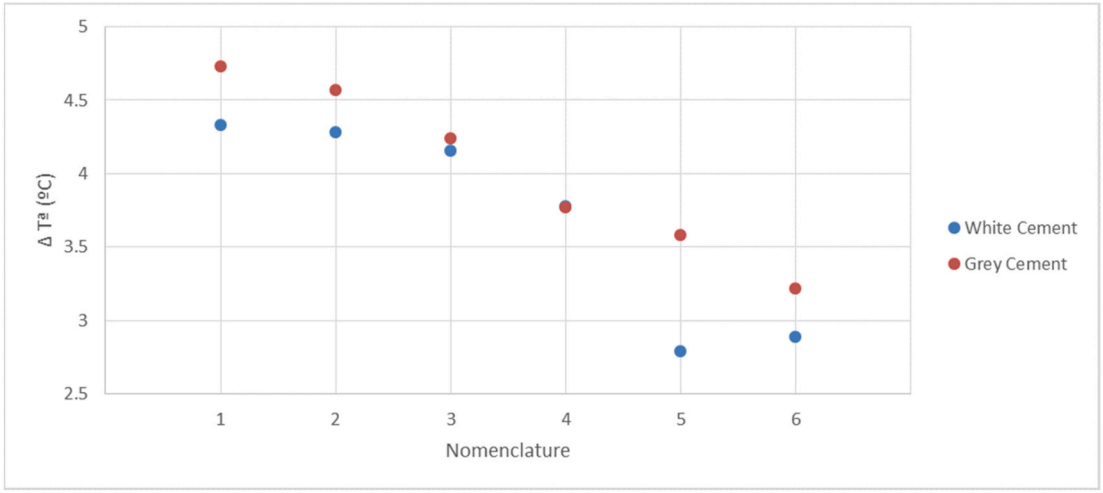

Fig. 10. Temperature increments (°C) for Full ROI of each cement.

3.4. Thermal conductivity test

3.4.1. Tests setup

The 12 mixtures evaluated in this work were accordingly drilled with the aim of introducing the RK-3 needle and measuring the thermal conductivity. During this process, it is important to ensure the contact between needle and tested material by placing thermal grease in the hole where the needle is situated (Blázquez et al., 2017a, 2017b). After the calibration of the sensor with the specific sample supplied by the manufacturer, three measurements were made on each sample to evaluate possible uncertainties.

It is also convenient to mention that, to obtain the most accurate data possible, ambient temperature was kept as constant as possible during the measurement process. Thus, to minimize these sources of error, about 15 min for samples and needle to equilibrate with the ambient temperature before taking measurements and around 15 min between readings for temperatures to equilibrate. Fig. 14 shows the drilling of the samples and the measuring process with TEMPOS.

3.4.2. Thermal conductivity results

As commented before, 3 thermal conductivity tests were carried out on each of the samples (6 specimens of grey cements and 6 specimens of white cements), so a total of 36 measurements were globally performed. After following the steps already described with the TEMPOS device, the thermal conductivity parameter was measured for each sample. These results, together with the deviation of each measuring are presented in Table 9 and Table 10.

As shown in the previous Tables 9 and 10, deviations are all below the usual acceptable values (±10%), and no abnormal values were detected. Analysing now the thermal conductivity results, it is possible to observe that, in general terms, white cement samples present higher conductivity values, but without notable differences with respect to the grey cement. In the case of this last group of specimens, it is clearly observable how the addition of pigment for its darkening (black pigment) contributes to decrease the thermal conductivity. Thus, the reference sample of this grey cement is the most thermally conductive of the set of samples analysed. Regarding the white cement samples, a small reduction in the thermal conductivity value is also observed in the first two samples (with a greater amount of black pigment), while the sample with only white pigment (W6) is the most conductive from a thermal point of view. Generally speaking, it can be established that the pigments do not have a significant influence on the thermal behaviour of

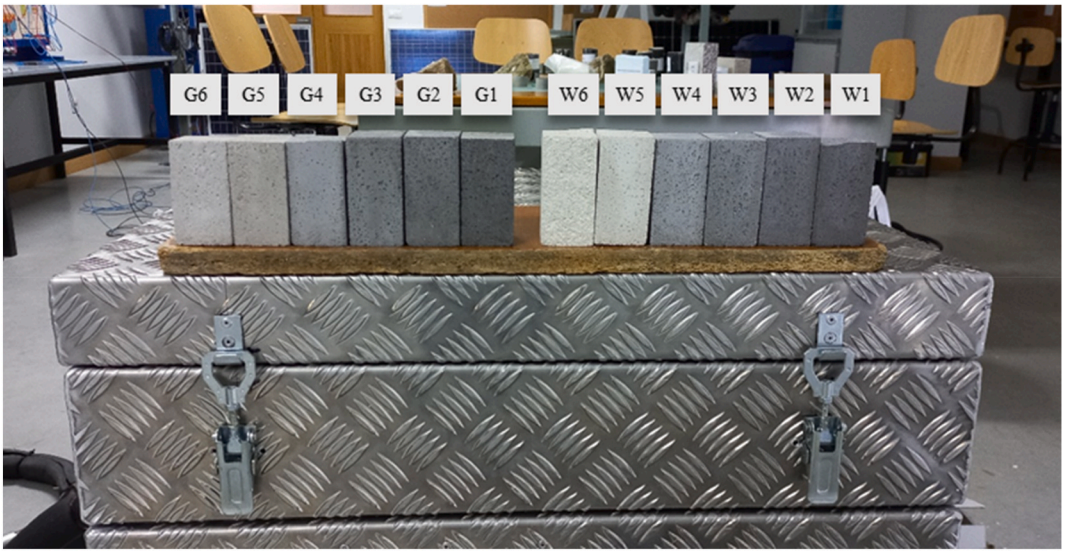

Fig. 11. Arrangement of the 12 mortar samples for the TLS data acquisition with the Faro Focus 3D 120. The 6 samples on the left correspond to the grey mortar samples and the 6 on the right correspond to the white mortar samples.

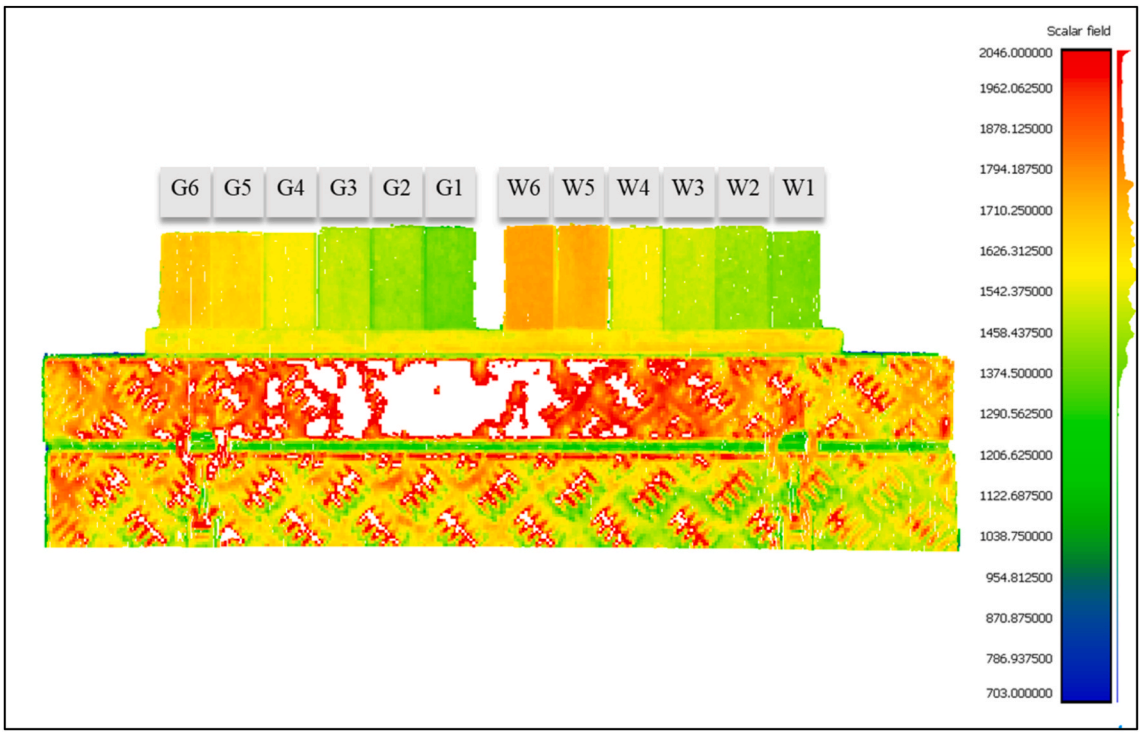

Fig. 12. Data acquired with the Faro Focus 3D 120: Point cloud with backscattered intensity values at 905 nm for the 12 mortar samples analysed.

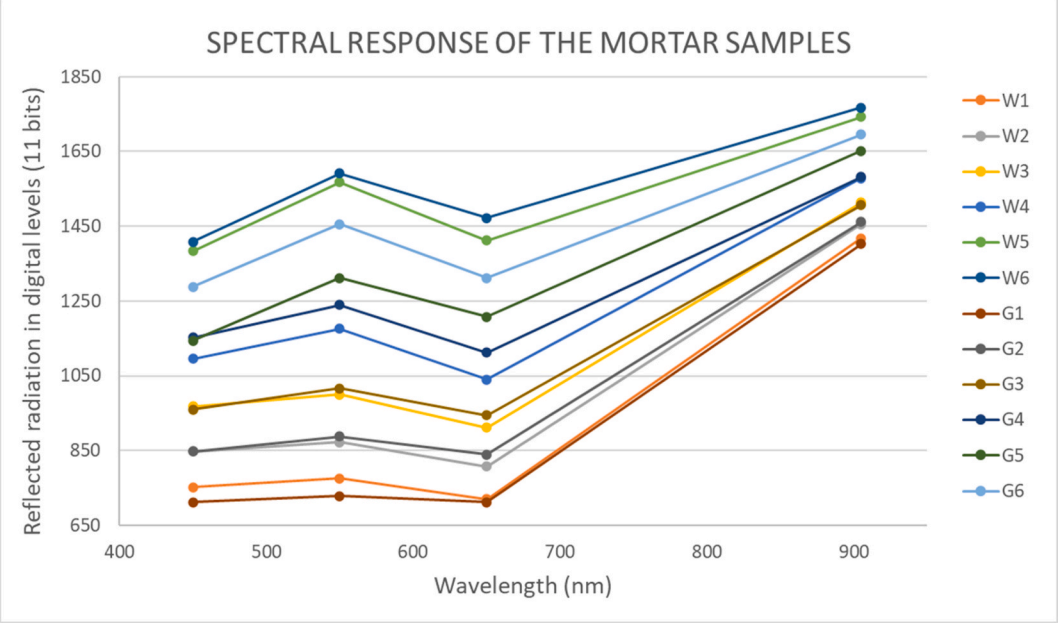

Fig. 13. Spectral response of the 12 mortar samples analysed for the VIS-NIR spectral range.

the tested materials, and that in any case, the trend is the reduction of the thermal conductivity with the addition of black pigment, especially in the grey cement samples. A slight increase in this thermal parameter could be also noticeable when white pigment is added, and black pigment is omitted.

4. Conclusions

This works aims at investigating the use of additive pigments to provide mortars with better thermal properties. To this end, two types of cement and six dosages with different proportions of pigment were evaluated by means of mechanical, thermal and optical tests.

First, the mechanical properties of each of the samples were analysed, which allowed us verifying that the addition of pigments in the percentages established by the manufacturer does not affect the compressive strength of the mortar. All the deviations found were within the limits established by the standards, which guarantees its use without modifying its performance.

The thermal heating tests of the samples showed that there are significant variations in the surface temperature reached at the different

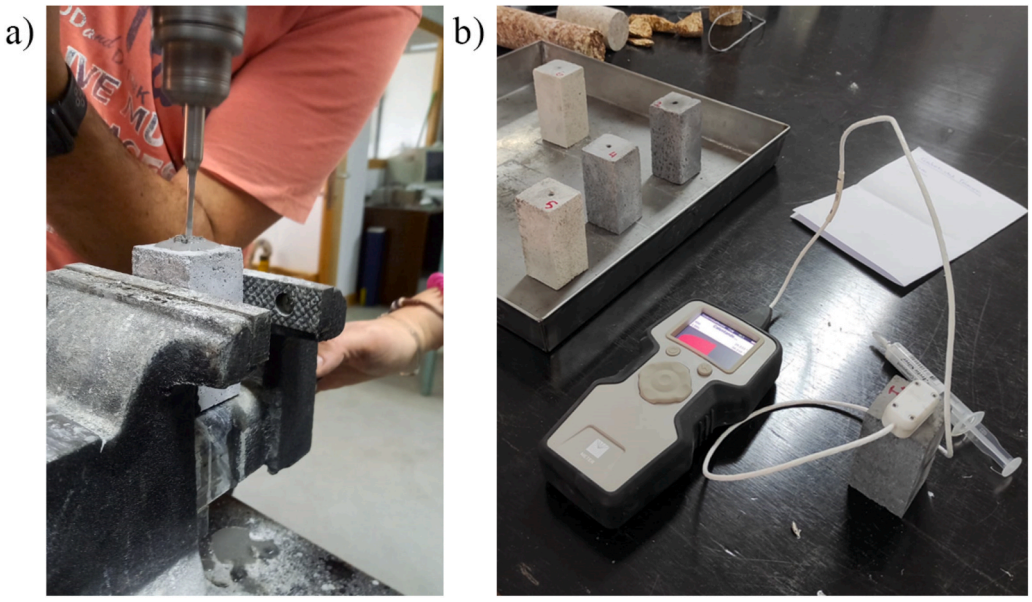

Fig. 14. Thermal conductivity test. a) Drilling; b) Measuring with TEMPOS and RK-3 needle.

Table 9
Thermal conductivity results obtained with TEMPOS for the Grey Cement.

Nomenclature	Measurement	Thermal Conductivity (W/m·K)	Deviation	Thermal Conductivity Average (W/m·K)	Deviation Average
G1	M-1	1.042	0.0035	1.041	0.0031
	M-2	1.121	0.0029		
	M-3	0.961	0.0029		
G2	M-1	1.242	0.0002	1.273	0.0003
	M-2	1.348	0.0003		
	M-3	1.230	0.0005		
G3	M-1	1.986	0.00036	1.884	0.0004
	M-2	1.876	0.00045		
	M-3	1.789	0.00040		
G4	M-1	1.419	0.021	1.363	0.022
	M-2	1.301	0.033		
	M-3	1.369	0.013		
G5-Ref	M-1	1.983	0.010	2.063	0.009
	M-2	1.996	0.008		
	M-3	2.211	0.0098		
G6	M-1	1.682	0.0001	1.626	0.0002
	M-2	1.594	0.0003		
	M-3	1.603	0.00025		

Table 10
Thermal conductivity results obtained with TEMPOS for the White Cement.

Nomenclature	Measurement	Thermal Conductivity (W/m·K)	Deviation	Thermal Conductivity Average (W/m·K)	Deviation Average
W1	M-1	1.593	0.003	1.596	0.003
	M-2	1.586	0.005		
	M-3	1.610	0.002		
W2	M-1	1.633	0.0007	1.621	0.0009
	M-2	1.549	0.0009		
	M-3	1.682	0.001		
W3	M-1	1.879	0.0002	1.918	0.0002
	M-2	1.967	0.0004		
	M-3	1.907	0.0001		
W4	M-1	1.739	0.0008	1.725	0.0007
	M-2	1.589	0.0009		
	M-3	1.846	0.0005		
W5-Ref	M-1	1.983	0.0007	1.774	0.009
	M-2	1.785	0.0009		
	M-3	1.554	0.001		
W6	M-1	1.959	0.002	2.103	0.001
	M-2	2.106	0.0005		
	M-3	2.243	0.0009		

dosages. On the one hand, WhPig hardly reduce the temperature of mortars, especially in the case of using WhC due to its high percentage of whiteness. Nevertheless, BlPig allow higher temperatures to be reached in the mortar samples. Thus, the surface temperature increases in those samples with the highest amount of BlPig. Specifically, it increases 32% with respect to the reference sample temperature in the case of GrC and 55% when using WhC. The rest of the samples containing BlPig also achieve a higher temperature rise, although the specific proportionality corresponding to the amount of pigment cannot be determined due to the mixing of two opposite colour pigments. In this sense, future work will focus on optimising similar pigments in different proportions in order to estimate the saturation point beyond which there is no significant temperature increase for an increase in pigment.

The optical reflectivity test showed a higher reflected radiation in the VIS and NIR for mortars with WhPig, i.e., mortars with BlPig have a higher radiation absorption. This behaviour agrees with the results obtained in the thermal analyses described above.

Finally, thermal conductivity tests were carried out in which small differences were found, showing that the effect of the pigments is very slight. Nevertheless, a lower thermal conductivity was found for samples with BlPig corresponding to GrC, while mortars with WhPig corresponding to WhC showed a higher thermal conductivity. This behaviour would help to reinforce the idea that the darker samples allow a higher temperature to be reached and stored while the whiter samples reach a lower temperature and could dissipate it earlier due to the higher thermal conductivity.

The results obtained for thermal behaviour highlight the high influence of the use of pigments, which could be useful for energy efficiency and heat storage functions such as solar chimneys or hot water tanks. Future work will focus on carrying out studies under real solar conditions and testing the effect of this increase in surface temperature on indoor fluids such as air or water.

CRediT authorship contribution statement

Jorge López-Rebollo: Methodology, Investigation, Formal analysis, Writing – original draft, Writing – review & editing. **Susana Del Pozo:** Conceptualization, Investigation, Formal analysis, Writing – review & editing. **Ignacio Martín Nieto:** Investigation, Formal analysis, Writing – review & editing. **Cristina Sáez Blázquez:** Investigation, Formal analysis, Writing – review & editing. **Diego González-Aguilera:** Supervision, Funding acquisition, Writing – review & editing.

Declaration of competing interest

The authors declare that they have no known competing financial interests or personal relationships that could have appeared to influence the work reported in this paper.

Data availability

Data will be made available on request.

Acknowledgements

The authors want to thank the Spanish Ministry of Education, Culture and Sports for providing an FPU grant (Training Program for Academic Staff) to the corresponding author of this paper (grant number FPU20/01376). This work was financed by ERDF funds and Junta of Castilla y León through the TCUE 2021–2023 program within the framework of the DACHARAP project (N° Ref. PC-TCUE21-23_033).

References

AENOR. UNE-EN 196-1. Methods of testing cement - Part 1: Determination of strength. Madrid, Spain2018.

Badin, G., Ahmad, N., Ali, H.M., 2020. Experimental investigation into the thermal augmentation of pigmented asphalt. Phys. Stat. Mech. Appl. 551, 123974 0378-4371.

Badin, G., Ahmad, N., Ali, H.M., Ahmad, T., Jameel, M.S., 2021. Effect of addition of pigments on thermal characteristics and the resulting performance enhancement of asphalt. Construct. Build. Mater. 302, 124212, 0950-0618.

Basha, S.I., Ali, M.R., Al-Dulaijan, S.U., Maslehuddin, M., 2020. Mechanical and thermal properties of lightweight recycled plastic aggregate concrete. J. Build. Eng. 32, 101710 2352-7102.

Berktas, I., Ghafar, A.N., Fontana, P., Caputcu, A., Menceloglu, Y., Okan, B.S., 2020. Facile synthesis of graphene from waste tire/silica hybrid additives and optimization study for the fabrication of thermally enhanced cement grouts. Molecules 25, 886.

Blázquez, C.S., Martín, A.F., Nieto, I.M., García, P.C., Pérez, L.S.S., Aguilera, D.G., 2017a. Thermal conductivity map of the Avila region (Spain) based on thermal conductivity measurements of different rock and soil samples, 71 0375 Geothermics 65, 60–6505.

Blázquez, C.S., Martín, A.F., Nieto, I.M., García, P.C., Pérez, L.S.S., González-Aguilera, D., 2017b. Analysis and study of different grouting materials in vertical geothermal closed-loop systems. Renew. Energy 114, 1189–1200, 0960-1481.

Bonifazi, G., Palmieri, R., Serranti, S., 2018. Evaluation of attached mortar on recycled concrete aggregates by hyperspectral imaging. Construct. Build. Mater. 169, 835-42 0950-618.

Carslaw, H.S., Jaeger, J.C., 1959. Conduction of Heat in Solids. Clarendon press.

Cellat, K., Tezcan, F., Kardaş, G., Paksoy, H., 2019. Comprehensive investigation of butyl stearate as a multifunctional smart concrete additive for energy-efficient buildings. Int. J. Energy Res. 43, 7146, 58 0363-907X.

Codd, D.S., Carlson, A., Rees, J., Slocum, A.H., 2010. A low cost high flux solar simulator. Sol. Energy 84, 2202–2212, 0038-092X.

Colarossi, D., Tagliolini, E., Principi, P., Fioretti, R., 2021. Design and validation of an adjustable large-scale solar simulator. Appl. Sci. 11, 1964.

Corinaldesi, V., Mazzoli, A., Moriconi, G., 2011. Mechanical behaviour and thermal conductivity of mortars containing waste rubber particles, 50 0261 Mater. Des. 32, 1646–3069.

Corinaldesi, V., Monosi, S., Ruello, M.L., 2012. Influence of inorganic pigments' addition on the performance of coloured SCC. Construct. Build. Mater. 30, 289–293, 0950-618.

Deilami, K., Kamruzzaman, M., Liu, Y., 2018. Urban heat island effect: a systematic review of spatio-temporal factors, data, methods, and mitigation measures. Int. J. Appl. Earth Obs. Geoinf. 67, 30, 42 0303-2434.

Del Pozo, S., Herrero-Pascual, J., Felipe-García, B., Hernández-López, D., Rodríguez-Gonzálvez, P., González-Aguilera, D., 2016. Multispectral radiometric analysis of façades to detect pathologies from active and passive remote sensing. Rem. Sens. 8, 80 2072-4292.

Divya, S., Das, S., 2021. New red pigments based on Li3AlMnO5 for NIR reflective cool coatings. Ceram. Int. 47, 30381, 30390 0272-8842.

Florian L. Interlacing the Evaluation of Mechanical Properties of Mortar Cement with Near-Infrared Spectroscopy Using Multivariate Data Analysis 2022.

George, M., Pandey, A.K., Abd Rahim, N., Tyagi, V.V., Shahabuddin, S., Saidur, R., 2020. A novel polyaniline (PANI)/paraffin wax nano composite phase change material: superior transition heat storage capacity, thermal conductivity and thermal reliability. Sol. Energy 204, 448–458, 0038-092X.

Gupta, A., Naval, S., 2020. A critical literature on auto repair behaviour of bio concrete. LIAST [International Journal of Advanced Science and Technology 29, 2043–2047.

Healy, J.J., De Groot, J.J., Kestin, J., 1976. The theory of the transient hot-wire method for measuring thermal conductivity, 408 0378 Phys. B+C 82, 392–4363.

Heerah, M.Z., Galobardes, I., Dawson, G., 2021. Characterisation and control of cementitious mixes with colour pigment admixtures. Case Stud. Constr. Mater. 15 e00571 2214-5095.

Lizaranzu, M., Lario, A., Chiminelli, A., Amenabar, I., 2015. Non-destructive testing of composite materials by means of active thermography-based tools, 20 1350 Infrared Phys. Technol. 71, 113–4495.

Lockmuller, N., Redgrove, J., Kubicar, L., 2004. Measurement of thermal conductivity with the needle probe, 38 0018 High. Temp. - High. Press. 36, 127–1544.

Maldague, X., 2001. Theory and Practice of Infrared Technology for Nondestructive Testing.

Matias, G., Torres, I., Rei, F., Gomes, F., 2020. Analysis of the functional performance of different mortars with incorporated residues. J. Build. Eng. 29, 101150 2352-7102.

Meng, Q., Wang, Y., Zhang, L., 2011. Irradiance characteristics and optimization design of a large-scale solar simulator. Sol. Energy 85, 1758–1767, 0038-092X.

Nocuń-Wczelik, W., Stolarska, K., 2019. Calorimetry in the studies of by-pass cement kiln dust as an additive to the calcium aluminate cement. J. Therm. Anal. Calorim. 138, 4561, 9 1588-2926.

PublicLab. Ultraviolet spectrometry. https://publiclab.org/wiki/uv-spectrometry. (Accessed 3 July 2022).

Puesan, C.-W.P., Mestre, J.-L.Z., 2017. Technical evaluation of an improved paint coating with NIR pigments designed to reduce thermal discomfort caused by incident solar radiation: application in the Caribbean area, 79 1876 Energy Proc. 115, 463–6102.

Reuben, N.O., Perez, P.A., Josiah, M.A., Abdul, M.M., 2018. Towards enhancing sustainable reuse of pre-treated drill cuttings for construction purposes by near-infrared analysis: a review, 39 2141 J. Civ. Eng. Construct. Technol. 9, 19–634.

Rodriguez-Gonzalvez, P., Gonzalez-Aguilera, D., Gonzalez-Jorge, H., Hernandez-Lopez, D., 2015. Low-cost reflectance-based method for the radiometric calibration of kinect 2. IEEE Sensor. J. 16, 1975, 1985 530-437X.

Rosati, A., Fedel, M., Rossi, S., 2021. NIR reflective pigments for cool roof applications: a comprehensive review. J. Clean. Prod. 313, 127826, 0959-6526.

Sánchez-Aparicio, L.J., Del Pozo, S., Ramos, L.F., Arce, A., Fernandes, F.M., 2018. Heritage site preservation with combined radiometric and geometric analysis of TLS data, 39 0926 Autom. ConStruct. 85, 24–5805.

Santos, B.O., Valença, J., Júlio, E., 2018. Classification of Biological Colonization on Concrete Surfaces Using False Colour HSV Images, Including Near-Infrared Information. SPIE, pp. 13–22.

Sukontasukkul, P., Uthaichotirat, P., Sangpet, T., Sisomphon, K., Newlands, M., Siripanichgorn, A., et al., 2019. Thermal properties of lightweight concrete incorporating high contents of phase change materials. Construct. Build. Mater. 207, 431–439, 0950-618.

Tawfik, M., Tonnellier, X., Sansom, C., 2018. Light source selection for a solar simulator for thermal applications: a review. Renew. Sustain. Energy Rev. 90, 802, 13 1364-0321.

Teijón-López-Zuazo, E., López-Rebollo, J., Sánchez-Aparicio, L.J., Garcia-Martín, R., Gonzalez-Aguilera, D., 2021. Compression and strain predictive models in non-structural recycled concretes made from construction and demolition wastes. Materials 14, 3177.

Thejus, P.K., Krishnapriya, K.V., Nishanth, K.G., 2021. NIR reflective, anticorrosive magenta pigment for energy saving sustainable building coatings. Sol. Energy 222, 103–114, 0038-092X.

Verian, K.P., Ashraf, W., Cao, Y., 2018. Properties of recycled concrete aggregate and their influence in new concrete production. Resour. Conserv. Recycl. 133, 30, 49 0921-3449.

Watanabe, A., Furukawa, H., Miyamoto, S., Minagawa, H., 2019. Non-destructive chemical analysis of water and chlorine content in cement paste using near-infrared spectroscopy. Construct. Build. Mater. 196, 95, 104 0950-618.

Xaman, J., Vargas-Lopez, R., Gijon-Rivera, M., Zavala-Guillen, I., Jimenez, M.J., Arce, J., 2019. Transient thermal analysis of a solar chimney for buildings with three different types of absorbing materials: copper plate/PCM/concrete wall. Renew. Energy 136, 139–158, 0960-1481.

Yun, T.S., Jeong, Y.J., Han, T.-S., Youm, K.-S., 2013. Evaluation of thermal conductivity for thermally insulated concretes, 32 0378 Energy Build. 61, 125–7788.